1 Fossil coccolith morphological attributes as a new proxy for deep
2 ocean carbonate chemistry

3 ~~Responses of fossil coccolith morphology to preservation~~
4 ~~conditions in the deep ocean~~

5 Authors: Amanda Gerotto[1,3]*, Hongrui Zhang[2]*, Renata Hanae Nagai[3], Heather M. Stoll[2], Rubens
6 César Lopes Figueira[1], Chuanlian Liu[4], Iván Hernández-Almeida[2]

7 [1]Oceanographic Institute, University of São Paulo, São Paulo, Brazil; [2]Geological Institute, ETH
8 Zurich, Zurich, Switzerland; [3]Center for Marine Studies, Federal University of Paraná, Pontal do
9 Paraná, Brazil; [4]State Key Laboratory of Marine Geology, Tongji University, Shanghai, China.

10 *Corresponding authors: gerottoamanda@alumni.usp.br, zhh@ethz.ch

12   Abstract

13 Understanding the variations in past ocean carbonate chemistry is critical ~~in~~ to elucidating the
14 role of the oceans in balancing the global carbon cycle. The fossil shells from marine calcifiers
15 present in the sedimentary record are widely applied as past ocean carbon cycle proxies.
16 However, the interpretation of these records can be challenging due to the complex~~ity~~
17 physiological and ecological response to the carbonate system during an organisms' life cycle,
18 as well as the potential for preservation at the sea~~-~~floor. Here we present a new dissolution
19 proxy based on the morphological attributes of coccolithophores from the Noëlaerhabdaceae
20 family (*Emiliania huxleyi* and *Gephyrocapsa* spp., > 2 μm). To evaluate the influences of
21 coccolithophore calcification and coccolith preservation on fossil morphology, we measured
22 morphological attributes, mass, length, thickness, and shape factor (ks), of coccoliths in a
23 laboratory dissolution experiment and surface sediment samples ~~in~~ from the South China Sea.
24 The coccolith morphological data in surface sediments were also analyzed with environment
25 settings, namely surface temperature, nutrients, pH, chlorophyll-a concentration, and carbonate
26 saturation of bottom water by a redundancy analysis. Statistical analysis indicates that
27 carbonate saturation of the deep ocean explains the highest proportion of variation in the
28 morphological data instead of the environmental variables of the surface ocean. Moreover, the
29 dissolution trajectory in the ks *vs.* length of coccoliths is comparable between natural samples
30 and laboratory dissolution experiments, emphasizing the importance of carbonate saturation
31 on fossil coccolith morphology. However, the mean ks alone cannot fully explain all variations
32 observed in our work. We propose that the mean ks and standard deviation of ks (σ) over the
33 mean ks (σ/ks) could reflect different degrees of dissolution and size-selective dissolution,

34 influenced by the assemblage composition. By applying together with the σ/ks ratio, the ks

35 factor of fossil coccoliths in deep ocean sediments could be a potential proxy for a quantitative

36 reconstruction of past carbonate dissolution dynamics.

37

1. Introduction

39 The ocean's large reservoir capacity of carbon dioxide (CO_2) plays an essential role in the

40 carbon cycle and, consequently, in controlling atmospheric CO_2 (Ridgwell and Zeebe, 2005;

41 Wang et al., 2016). The ocean ~~p~~CO_2 is influenced by temperature, salinity, and biological activity,

42 including primary production, respiration, calcification, and carbonate dissolution (Ridgwell and

43 Zeebe, 2005; Sarmiento and Gruber, 2006; Libes, 2009; Wang et al., 2016). When CO_2 dissolves

44 in water, the ocean becomes more acidic, decreasing pH, carbonate ion concentration, and

45 carbonate saturation (Ω_{Ca}). The carbonate compensation depth (CCD) is the depth at which the

46 rate of calcite dissolution is balanced by the rate of calcite supply. The CCD is usually several

47 hundred meters deeper than the chemical lysocline, the saturation horizon of calcite, due to the

48 kinetics of dissolution (Ridgwell and Zeebe, 2005). Whereas the photic zone is supersaturated

49 with respect to calcite in most areas of the ocean, large areas of the deep ocean are currently

50 undersaturated because of the increased solubility of calcite with pressure (Sulpis et al., 2018).

51 As the ocean continues absorbing larger amounts of CO_2 from anthropogenic fuel emissions, a

52 shallowing of the CCD is expected for the next 100 years due to the sharp decrease of carbonate

53 saturation from surface to deep ocean (Hönisch et al., 2012; USGCRP, 2017; Sulpis et al., 2018;

54 IPCC, 2019). Variations in the CCD on timescales from millions to several thousands of years are

55 an important process in determining the ocean's carbonate chemistry and regulating

56 atmospheric CO_2 (Emerson and Archer, 1990; Pälike et al., 2006). Understanding the role of

57 physical and biogeochemical parameters in marine carbonates is therefore critical to interpret

58 the geological record correctly and to reconstruct variations ~~of~~ in the ocean carbon cycle in the

59 past.

60 The effects of carbonate chemistry changes and variations in the position of the CCD in

61 the geological past have been investigated using a wide array of geochemical and microfossil

62 proxies such as $\delta^{13}C$ in benthic and planktonic foraminifera (Zachos et al., 2005; Hönisch et al.,

63 2012), fragmentation indices of calcareous microfossils (Le and Shackleton, 1992; Broerse et al.,

64 2000; Flores et al., 2003), and $CaCO_3$ content (Archer et al., 2000; Palike et al., 2006) in marine

65 sediments. However, these proxies do not provide quantitative estimates of past changes in

66 carbonate chemistry because some additional ecological mechanisms determine the

67 calcification and preservation responses (Hönisch et al., 2012; Rae et al., 2021). $\delta^{11}B$ provides a

68   quantitative proxy for past seawater pH (Hönisch et al., 2012), albeit additional carbonate

69   chemistry parameters impose some limits on the interpretation of the proxy (Yu and Elderfield,

70   2007; Rae et al., 2021). Benthic B/Ca provides a quantitative proxy for deep sea CO_3^{-2}

71   concentration (Yu et al., 2016). Yet both of these methods require mono-specific foraminifera

72   samples for measurements, which are time-consuming to pick, and analyses are limited to

73   sediment samples that contain sufficient concentration of this microfossil group.

74   Coccolithophores, a group of single-celled calcifying algae, are characterized by the

75   production of calcite plates called coccoliths. Coccoliths are the main constituent of marine

76   biogenic sediments, contributing up to 80 % ~~to~~ of deep-sea carbonate fluxes (Young and Ziveri,

77   2000; Hay, 2004). Changes in coccoliths morphology, distribution, and abundances ~~were~~ are

78   believed to record the evolution history of coccolithophores and reflect the environmental

79   conditions in the surface ocean (i.e. during coccolith biomineralization) (Riebesell et al., 2000;

80   Iglesias-Rodriguez et al., 2008; Beaufort et al., 2011; Charalampopoulou et al., 2016; Rigual-

81   Hernández et al., 2020a). Because of that, coccoliths are widely used in paleoclimate and

82   paleoceanographic reconstructions (e.g., Bollman and Herrle, 2007; Rickaby et al., 2007;

83   Henderiks and Pagani, 2007; Bolton et al., 2016~~; Bollman and Herrle, 2007~~). Several methods

84   exist to estimate coccolithophore calcification in the fossil record. Assumed proportional length

85   and thickness allowed for the first estimates of coccolith mass using microscope techniques

86   (Young and Ziveri, 2000). More recent methods based on the optical properties of calcite under

87   polarized light microscopy (circular and linear) allowed a more precise estimate of the thickness

88   of individual coccoliths (Beaufort, 2005; ~~Beaufort et al., 2021;~~ Bollman et al., 2014; Fuertes et

89   al., 2014; Johnsen and Bollmann, 2020; Beaufort et al., 2021). The optical techniques have been

90   successfully employed in downcore records to estimate coccolithophore calcification across

91   time and evolutionary steps (e.g., Bolton et al., 2016; Beaufort et al., 2022; Guitián et al., 2022).

92   However, until now there ~~is~~ has been no study that evaluates the response of calcification

93   patterns of fossil coccolithophores to both environmental parameters controlling

94   biomineralization in the photic zone and calcite saturation state at the depth of burial.

95   The South China Sea (SCS) is the largest marginal basin of the Western Pacific,

96   characterized by very dynamic spatial environmental conditions and a steep bathymetric profile

97   (Wang et al., 2015). Sediment records from this basin have been used to study the response of

98   coccolithophores to different environmental variables. Previous studies found positive

99   correlations between coccolithophore~~s~~ biometry from plankton samples and nutrients and light

100   at the photic zone (Jin et al., 2016). Building ~~up~~ on these results, but applied to the sedimentary

101   record, Su et al. (2020) explored the dependency of coccolithophore weight and past surface

102   ocean carbon chemistry parameters and nutrient conditions. However, it has also been ~~also~~

demonstrated that there is intense coccolithophore dissolution above the lysocline in the SCS (Fernando et al., 2007a). More recently, a study using plankton tow material found that the degree of calcification in the coccolithophore species *Emiliania huxleyi* was insensitive to carbonate chemistry in surface waters (Jin et al. 2022a). This diversity of results calls for new studies that ~~explore~~ systematically explore the drivers of coccolithophore morphology and calcification in the fossil record.

Here, we analyzed morphological attributes of fossil coccolithophores in surface sediment samples ~~(n = 28)~~ in the SCS, located across spatial environmental gradients in the surface ocean, but also across a bathymetric transect related to the calcite saturation at the seafloor ~~floor~~ which leads to lower calcite saturation at the sea-floor in deeper sites. In addition, we evaluated the morphological variations of coccoliths under different dissolution intensities in a laboratory experiment. Using an automated algorithm to estimate coccolithophore calcification from images taken with a microscope under cross-polarization, we show that scale-invariant measures of coccolith thickness (shape factor, ks) from coccolithophores located along a depth gradient in the SCS are highly correlated to the calcite saturation state at the seafloor. We propose a new calibration to reconstruct past calcite saturation based on ks which would enable the quantitative reconstruction of changes in the calcite saturation in the deep ocean and position of the CCD in the past.

2. Oceanographic settings

The SCS is a marginal basin located in the Western Pacific, connected to the open ocean by ~~north and south~~ shallow passages to the north and south (Fig. 1A). The Luzon Strait in the north is the deepest (~2000 m) and the principal channel for water exchange~~s~~ between the SCS and the Pacific through the Kuroshio Current (Qu et al., 2006; Liu et al., 2011; Wan and Jian, 2014). The modern surface circulation and hydrographic characteristics of the SCS are directly associated with the seasonal changes promoted by the East Asian Monsoon (EAM; Wang and Li, 2009). These seasonal hydrodynamic patterns control the regional sea surface temperature (SST) distribution, salinity, and nutrients (Fig. 1B-E, Wang and Li, 2009). The SST latitudinal gradient is up to 2° C with an annual average of 28-29° C in the southern SCS and 26-27° C in the north (Tian et al., 2010). Salinity varies seasonally between 32.8-34.2 psu, with smaller salinity variation in the north than in the south (Wang and Li, 2009). Northern SCS primary productivity reflects the seasonality of the EAM with more productive and well-mixed waters during the winter season (Zhang et al., 2016), with higher chlorophyll-*a* concentration (0.65 mg Chl-α m^{-3} and 600 mg C m^{-2} d^{-1}) (Chen, 2005; Chen et al., 2006; Jin et al., 2016).

139
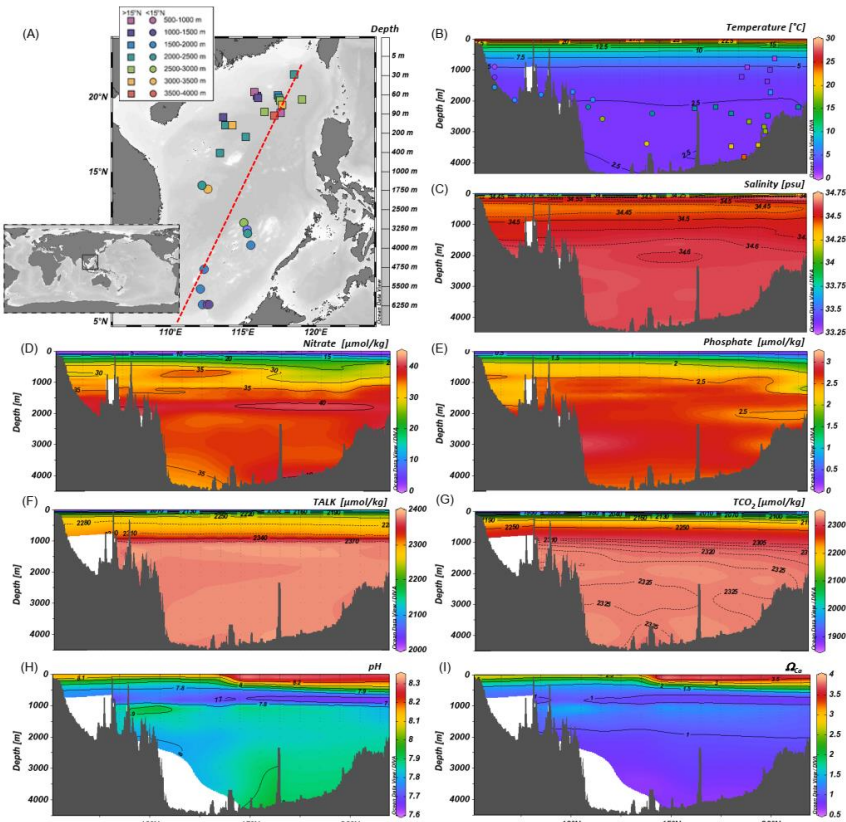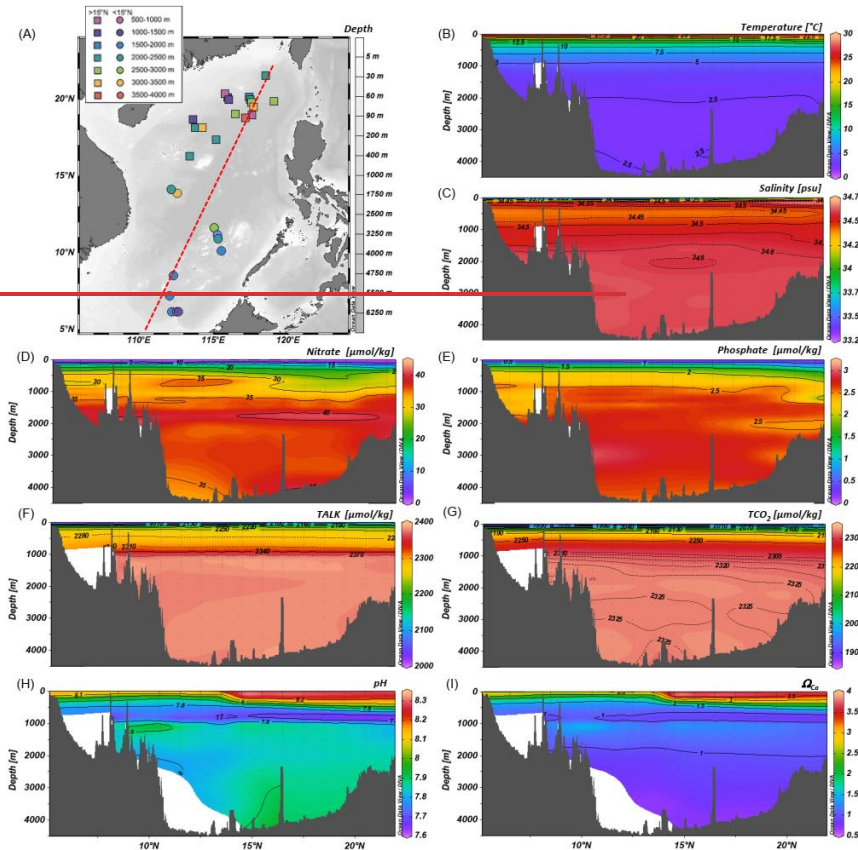
140 Figure 1. Map of the South China Sea and location of core-top samples used in the present study.

141 Dots and squares represent stations located from 6° to 15° N, and from 15° to 22° N. (A). Vertical

142 profiles along N-S (5° to 22° N) transect (dotted red line on panel A) of (B) temperature, (C)

143 salinity, (D) nitrate, and (E) phosphate obtained from World Ocean Atlas 2001 (WOA01,

144 Conkright et al., 2002), (F) total alkalinity (TALK) and (G) total inorganic carbon concentration

145 (TCO_2) from Goyet et al. (2000), (H) pH and (I) Ω_{Ca} calculated at CO2SYS (Pierrot et al., 2012)

146 from previously extracted data (Goyet et al., 2000). See M&M 3.3 section for data sources. The

147 map and the vertical profiles were plotted with Ocean Data View (ODV) software (Schlitzer,

148 2019). Colored dots in panel (B) indicate the geographical position along the transect shown in

149 panel (A) of the surface sediment samples used in this study.

150

151 The modern SCS lysocline is approximately 1200 m, and the CCD lies between 3500 and

152 3800 m (Thunell et al., 1992; Wang et al., 1995; Luo et al., 2018). In the northern SCS, surface

153 waters (e.g., the upper 300 m) are characterized by relatively lower DIC and TALK (Fig. 1F-G) and

154 higher pH and Ω_{Ca}, compared to deeper waters (Fig. 1H-I) (Chou et al., 2007; Jin et al., 2016).

155 Below 1000 m, the SCS across a N-S transect is characterized by relatively homogeneous DIC,

156 $\delta^{13}C$, and $[CO_3^{2-}]$ (Chen et al., 2006; Qu et al., 2006; Chou et al., 2007; Wan et al., 2020).

157 The SCS deep waters originate from the North Pacific Deep Water (NPDW) that

158 penetrates the marginal basin through the Luzon Strait (Qu et al., 2006; Liu et al., 2011; Wan

159 and Jian, 2014; Wan et al., 2018). The route traced from the Luzon Strait to the northwest

160 suggests a predominantly cyclonic deep circulation (Qu et al., 2006; Wang and Li, 2009). The

161 deep-water residence time of the SCS is estimated to be approximately 30-50 years, like that of

162 intermediate waters, 52 years (Chen et al., 2001). Due to this short residence time, the SCS

163 presents a homogeneous vertical profile; below 2000 m, there are no evident chemical

164 stratification or changes compared to the Pacific deep-water chemistry (> 2000 m)

165 characteristics (Chen et al., 2001; 2006; Qu et al., 2009). The rapid residence time potentially

166 implies that, when replaced, deep waters occupy intermediate water levels (between 300 m and

167 1300 m), contributing to the circulation of intermediate and shallow waters and ocean-

168 atmosphere exchanges (Qu et al., 2009; Tian et al., 2010).

3. Material and methods

3.1 Material and sample treatments

171 The core-top samples (n =28) employed in this study were retrieved from different

172 depths in the basin of SCS (Fig. 1) during the R/V Sonne cruises (SO-95) (Table 1). Toothpick

173 samples from each location were used to prepare smear slides, without any chemical or physical

174 treatment, following standard micropaleontological procedures (Marsaglia et al., 2015).

175 Unfortunately, the surface sediments were already depleted resulting in not having enough

176 material to perform dissolution experiments using the same samples. For the dissolution

177 experiment, we employed 240 mg of dry sediment obtained from the a Late Pleistocene sample

178 from the Western Equatorial Pacific (Ocean Drilling Program -ODP- 807A-2H-2W, 57-59 cm). The

179 distribution of coccolithophore species belonging to the Noëlaerhabdaceae family in the sample

180 ODP 807 is 41% of *G. oceanica*, 34% of *G. caribbeanica* and 23% of small *Gephyrocapsa*. These

181 taxa are thicker particularly *G. caribbeanica,* than the thinner Noëlaerhabdaceae species

182 commonly found in the SCS (e.g. *E. huxleyi,* Roth and Berger, 1975; Roth and Coulbourn, 1982).

183 The sediment sample was suspended in 120 ml Milli-Q water, and then the suspension was

184 evenly separated into 6 centrifuge tubes, each with a volume of 20 mL and containing the

185 equivalent of 40 mg of sediment. Sodium hexametaphosphate $(NaPO_3)_6$ (Calgon®) has been

186 traditionally been used in pretreatment of samples with calcareous microfossils, particularly

187   foraminifera (Olson and Smart 2004; Smart et al., 2008). However, it has been observed that
188   application of this chemical agent dissolves these microfossils due to complexation of Ca with
189   phosphates, an effect which varies with the exposure time (Feldmeijer et al., 2013). Therefore,
190   we added 100 mg of Calgon® into 100 ml Milli-Q water, resulting in a concentration of 1.6mM,
191   to conduct our dissolution experiment. Different volumes of Calgon® solution (0, 0.4, 0.8, 2, 4 6
192   ml) were added to each of the six subsamples. The Calgon® is very corrosive to the fine
193   carbonate particles, and the reaction between Calgon® and carbonate could be simplified in two
194   steps. First, the $(NaPO_3)_6$ hydrolysis releases the sodium trimetaphosphate $(Na_3P_3O_9)$. Then, the
195   calcium in the solution is exchanged with sodium and precipitate as $Ca(PO_3)_2$, $CaNa(PO_3)_3$, and
196    $CaNa_4(PO_3)_6$, strongly reducing the free calcium concentration in the solution. The decrease in
197   calcium concentration promotes carbonate dissolution. In theory, adding 1 mol $(NaPO_3)_6$ would
198   result in the dissolution of 3 mol $CaCO_3$ at maximum. So, there could be ~80 % carbonate left
199   even after adding 6 ml Calgon® solution. The particles in all tubes were kept suspended gently
200   by a rotating disaggregation wheel as described previously (Stoll and Ziveri, 2002) for two days
201   to achieve a full reaction between carbonate and $(NaPO_3)_6$. Slides were prepared for coccolith
202   morphological analyses using the drop technique as described by Bordiga et al. (2015) to trace
203   the variations of coccolith amount during dissolution.
204

205   3.2 Coccolith morphological parameters
206   The morphological parameters of coccoliths in the dissolution experiment and surface
207   sediment were analyzed using a Polarized Microscope (Zeiss Axio Scope HAL100), configured
208   with circularly polarized light and a Zeiss Plan-APOCHROMAT 100x/1.4 oil objective, and a
209   coupled camera (Zeiss Axiocam 506 Color). For every sample, at least 40 fields of view were
210   photographed. After species identification and selection of coccolithophores images belonging
211   to the Noëlaerhabdaceae family (*Emiliania huxleyi* and *Gephyrocapsa* spp., > 2 μm), each sample
212   had between 100 and 400 (average of 250 per sample) coccolithophore images. The relationship
213   between the color of coccolith images and thickness was calibrated using a reference calcite
214   wedge, the thickness of which had been carefully quantified (González-Lemos et al., 2018). After
215   calibration, all images were analyzed in the Matlab-based software, C-Calcita (Fuertes et al.,
216   2014), to obtain the coccolith morphological parameters, including length, volume, and mass.
217   The length-shape factor of each coccolith, ks, was calculated using the formulation by Young and
218   Ziveri (2000) based on the coccolith mass and length obtained using from C-Calcita:
219    $\text{ks} = \frac{Mass}{2.7 \times Length^3}$
220

221   Beyond the traditional morphological parameters, we calculated the ratio of the
222   standard deviation of ks (σ) over the mean ks (σ/ks). The goal of this novel parameter is to
223   provide a new dimension to trace the dissolution process in coccoliths, especially when the
224   coccolith assemblage is diverse. For example, if the coccoliths dissolve at different speeds in the
225   assemblage due to differential sensitivity to acidification, a small increase of σ/ks would be
226   expected at the beginning of the dissolution because of the σ increase and ks decrease. Then,
227   after all fragile coccoliths dissolve, leaving only thicker coccoliths in the assemblage, the σ/ks
228   should show a decreasing trend which could be mainly caused by a decrease σ.

229

230   Table 1. Station, coordinate data, and water depth of core-top samples used in this study.

Station	Longitude (E)	Latitude (N)	Water depth (m)
17930	115.782	20.333	629
17965	112.552	6.157	889
17943	117.553	18.95	917
17931	115.963	20.1	1005
17944	113.637	18.658	1219
17963	112.667	6.167	1233
17932	116.037	19.952	1365
17964	112.213	6.158	1556
17960	115.558	10.12	1707
17940	117.383	20.117	1728
17961	112.332	8.507	1795
17959	115.287	11.138	1957
17962	112.082	7.182	1970
17949	115.167	17.348	2195
17957	115.31	10.9	2197
17941	118.483	21.517	2201
17951	113.41	16.288	2340
17945	113.777	18.127	2404
17955	112.177	14.122	2404
17939	117.455	19.97	2473
17958	115.082	11.622	2581
17934	116.462	19.032	2665
17938	117.538	19.787	2835

17925	119.047	19.853	2980
17956	112.588	13.848	3387
17937	117.665	19.5	3428
17946	114.25	18.125	3465
17936	117.12	18.767	3809

231

232

233 3.3 Environmental data for surface sediment

234 Annual means of different physical, chemical and biological variables in both 50 m depth

235 and bottom water for the location of the surface samples (Table 1) were extracted from different

236 databases, interpolated to the geographical location of the surface sediment samples. Here the

237 50 m depth was selected because it is the depth at which the highest concentration of

238 Noëlaerhabdaceae coccolithophorid has beenis observed in the SCS (Jin et al., 2016). Seawater

239 temperature, salinity, nitrate, and phosphate, and nitrate concentrations at 50 m were obtained

240 from WOA01 (Fig. 1B,C,D,E). Sea surface chlorophyll-a concentration data were based on MODIS

241 data (2003-2016) extracted from Oregon State University Ocean Productivity

242 (http://www.science.oregonstate.edu/ocean.productivity/). Annual averaged concentrations of

243 total alkalinity (TALK) and dissolved inorganic carbon (TCO$_2$) were extracted from Goyet et al.

244 (2000) (Fig. 1F,G). Then the carbonate ion concentration, Ph (Fig. 1H), pCO$_2$ for the depth of 50

245 m and Ω_{Ca} for the sea-floor depth were calculated by CO2SYS macro for Excel® (Pierrot et al.,

246 2012) (Fig. 1I) using extracted variables, salinity, temperature, pressure, total phosphate, total

247 silicate, TALK, and TCO$_2$ at the corresponding depth (50 m or depth of the surface sediment

248 sample). The light intensity at 50 m water depth was calculated using a model of penetration of

249 photosynthetic active radiation (PAR) from surface to depth (Buiteveld, 1995; Murtugudde et

250 al., 2002), monthly climatologies of PAR from the MODIS Ocean database

251 (http://oceancolor.gsfc.nasa.gov/cgi/l3), and the diffuse attenuation coefficient for

252 downwelling irradiance at 490 nm (Kd490) and Equation 1 in Lin et al. (2016).

253

254 3.4 Statistical analysis

255 Pearson correlation and redundancy analysis (RDA) were employed to explore the

256 relationship between morphological features of the coccoliths in surface sediment samples and

257 the environmental data. All statistical analyses were performed using the PAST 4.06 software

258 (Hammer et al., 2001).

259

4. Results

4.1 Variations of coccoliths morphology in the dissolution experiment

In the dissolution experiment, mean ks decreased with increasing volume of Calgon® solution (Fig. 2A). The mean ks varied between 0.12 (0 ml Calgon®) and 0.04 (6 ml Calgon®) (Fig. 2A). The σ/ks represents variation in preservation among coccoliths within each sample. Higher differences in σ were observed in samples containing 2 ml, 4 ml, 0.8 ml, 0.4 ml, 0 ml, and 6 ml, respectively (Fig. 2B). Increasing the amount of Calgon® solution up to 2 ml showed a decrease in mean ks and an increase in σ. Samples with 4 and 6 ml Calgon® solution showed a reduction in mean ks and σ among coccoliths (Fig. 2B). The lowest mean ks (0.04) and the maximum mean length (3.95 µm) were recorded under the higher Calgon® solution (6 ml) amount (Fig. 2C). Increased amounts of Calgon® solution also resulted in a gradual increase in coccolith length leading to a negative correlation between length and ks (r= -0.68, p > 0.05), but not significant due to the small number of observations (Fig. 2C).
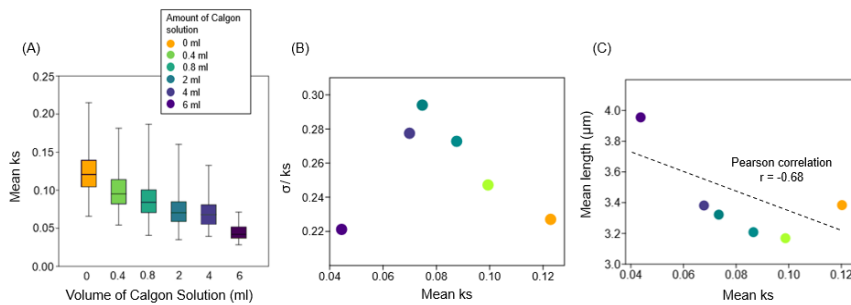
Figure 2. Coccolith morphological variations in the dissolution experiment. (A) Box plots of the median (horizontal line inside the boxes), minimal and maximal values of coccoliths mean ks (vertical bars) under the different volumes of Calgon® solution; (B) Scatter plot of mean ks and σ/ks and (C) linear correlation and correlation coefficient (p > 0.05) between mean ks and mean length.

4.2 ~~Morphological changes~~ Variations in coccolith morphology in natural conditions~~Biological and environmental effects on coccolith morphology~~

Overall, the mean ks, thickness, and volume in the core-top sampling stations (Fig. 3) presented higher values in shallower depths. The mean ks varied between 0.03 and 0.07, and the mean thickness was between 0.25 and 0.44 µm, with maximum values recorded at station 17931 located in northern SCS at 1005 m water depth. The mean length of coccolith varied between 3.23 and 3.78 µm, with the highest values recorded at 2195 m water depth (site 17949) in northern SCS, but without a significant trend along depths. The mean volume of coccoliths

288   ranged between 1.70 and 2.97 μm³, and the mean mass was between 4.61 and 8.03 pg, with

289   maximum values for both recorded in the shallowest station, (e.g. 17930), at 629 m water depth

290   in northern SCS.

291

292
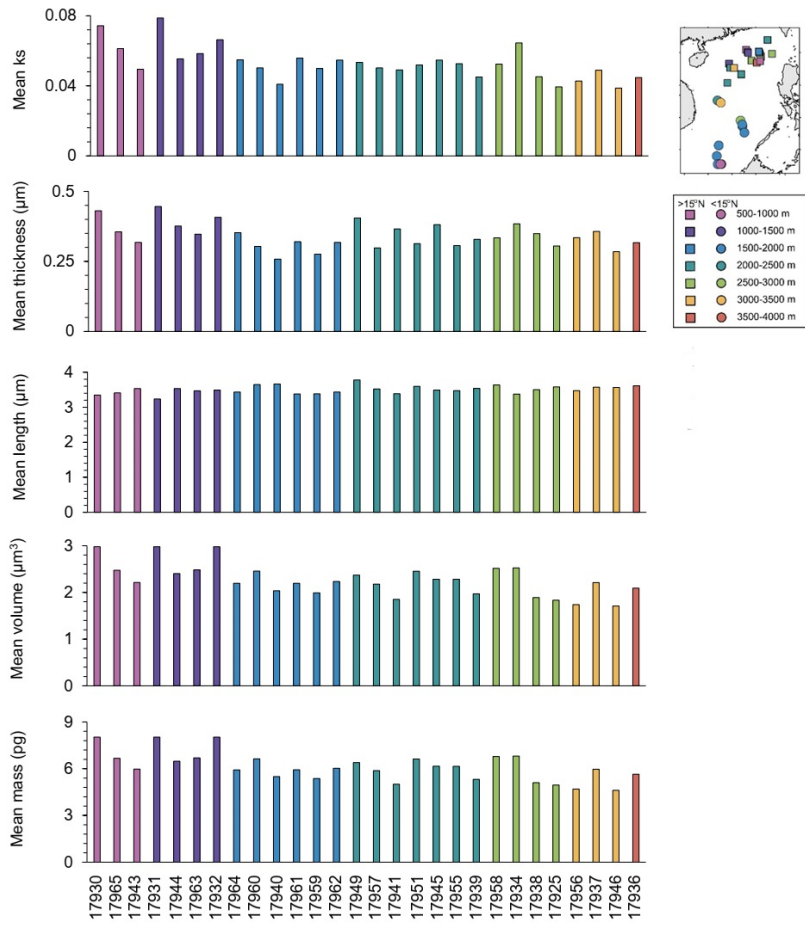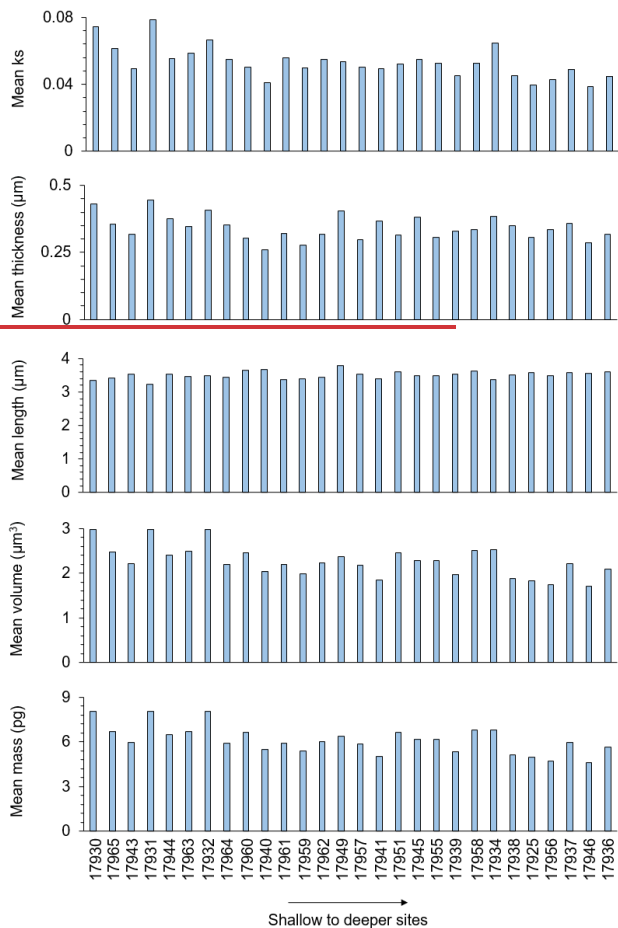
Figure 3. Coccolith mean ks, thickness (µm), length (µm), volume (µm^3), and mass (pg) in surface samples from SCS. The sampling stations are distributed along the x-axis according to their depth, sorted from the shallowest to the deepest.

296

In general, the degree of dissolution varied according to the depth of the sediment samples. The calcite saturation, Ω_{Ca}, decreases with colder temperature, higher pressure and higher CO_2 concentration in deep ocean.~~In general, the degree of dissolution varied according to the depth of the sediment samples.~~ The σ/ks *vs*. ks presents different trajectories associated with light, strong, or no dissolution (Fig. 4A). The shallowest stations south (<15˚ N) and north SCS (> 15˚ N) show a linear and increasing trend between ks and σ/ks. For the samples below 2000 m, there is no clear pattern of variation related to the mean ks standard deviation. However, samples below 3000 m are mainly located on the left upper part of the plot, in a similar

305 position as the samples treated with 4 and 6 ml of Calgon® in the ks *vs.* σ/ks comparison of the

306 dissolution experiment (Fig. 3B). The mean ks *vs.* mean length shows a negative correlation (r =

307 -0.62, p < 0.05), with the deepest samples showing larger size coccoliths and lower mean ks (Fig.

308 4B).

309

310

311
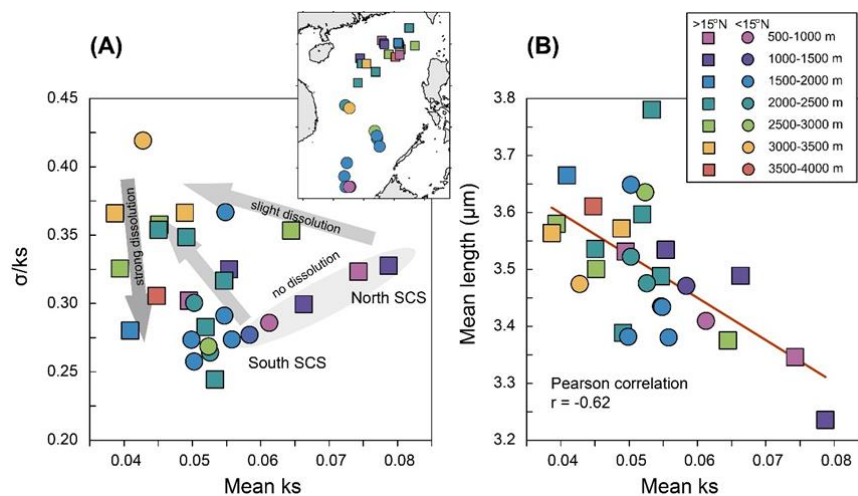
312 Figure 4. Morphological parameters of coccolith in surface sediments (A) Scatter plot between

313 mean ks and σ/ks and (B) linear correlation and correlation coefficient (p < 0.05) between mean

314 ks and mean length. Shaded arrows in panel A represent ideal trajectories of mean ks *vs.* σ/ks

315 as shown in figure 2B, to interpret the trends in the surface sediment samples. Note that the

316 mean ks of figures 2 and 4 are different due to the higher abundance of the species

317 ~~Gephyrocapsa~~ *G. caribbeanica,* with higher thickness, in the sample for the dissolution

318 experiment.

319

320 We analyzed the correlations between the biological and environmental datasets (Table

321 2). Although some of the surface variables were autocorrelated, they were included in our

322 analyses because some studies have identified a strong influence of these parameters on

323 coccolith morphology during the life-cycle (e.g. Chen et al., 2007; Jin et al., 2016). Significant

324 correlations can be found (p < 0.05) between several morphological parameters of coccolith and

325 bottom water carbonate chemistry (Ω_{Ca}), with a correlation coefficient (r) = 0.67 between mean

326 ks and Ω_{Ca}, r = 0.66 between mean volume and Ω_{Ca}, and r = 0.66 between mass and Ω_{Ca}. The

327 mean thickness of the coccolith shows a significant correlation with Ω_{Ca} at the sample depth (r

= 0.41), and with the concentrations of nutrients nitrate and phosphate at 50 m (r = 0.44 and 0.4, respectively). Surprisingly, the mean length showed no significant correlation to any environmental variables except with PAR (r = 0.35).

The results of RDA can provide another critical perspective on the control of environmental variables on coccolith morphology. The RDA1 and RDA2 explain together 58.3 % of the total variations in coccolith morphological data. The surface sediment samples, color-coded by different depth intervals, are distributed along the axis of RDA1, which is the most important and explains 54.6 % of the total variance (Fig. 5A). Among the environmental variables, Ω_{Ca} shows the highest correlation to RDA1 (r = -0.67, p < 0.05). The results of both the correlation analyses and the RDA show that Ω_{Ca} in bottom water is the most important environmental variable driving the morphological dataset, which shows a high correlation with mean ks (r= 0.69; p < 0.05) and could explain up to 47 % (R^2= 0.47) of the variance observed in mean ks (Fig. 5B). The RDA2 explained 3.69 % of the variance and is mainly correlated to the salinity, temperature, pH, phosphate, TALK, and pCO_2 (Fig. 5A). The null response of coccolith length to any environmental parameter is also observed in the RDA plot by its position near the center of the ordination space, significantly contrasting with other morphological parameters (Fig. 5A).

Table 2. Correlation matrix (p-value and Pearson correlation) between biological and environmental variables. Bold values indicate significant correlations (with p < 0.05).

Environmental/ Biological	p value					r				
	Mean ks	Mean thickness	Mean length	Mean volume	Mean mass	Mean ks	Mean thickness	Mean length	Mean volume	Mean mass
Salinity	0.79	0.07	0.87	0.86	0.86	-0.05	0.34	0.03	-0.03	-0.03
Temperature	0.94	0,04	1.0	0.90	0.90	-0.01	-0.39	0.00	-0.02	-0.02
Phosphate	0.88	0.03	0.63	0.96	0.96	0.03	**0.41**	-0.09	-0.01	-0.01
Nitrate	0.36	0.02	0.30	0.71	0.71	0.17	**0.44**	-0.20	0.07	0.07
TALK	0.53	0.13	0.70	0.60	0.60	-0.12	0.28	0.07	-0.10	-0.10
Chlorophyll-a	0.26	0.18	0.88	0.18	0.18	0.22	0.25	-0.02	0.26	0.26
PAR	0.28	0.05	0.06	0.50	0.50	-0.21	-0.38	0.35	-0.13	-0.13
pH	0.18	0.31	0.38	0.24	0.24	-0.26	0.19	0.17	-0.22	-0.22
pCO_2	0.16	0.33	0.38	0.21	0.21	0.27	-0.19	-0.17	0.24	0.24
Ω_{Ca}	**0.00**	**0.03**	0.05	**0.00**	**0.00**	**0.67**	**0.41**	-0.36	**0.66**	**0.66**

TALK = total alkalinity, PAR = photosynthetic active radiation and, Ω_{Ca} = carbonate saturation.

350
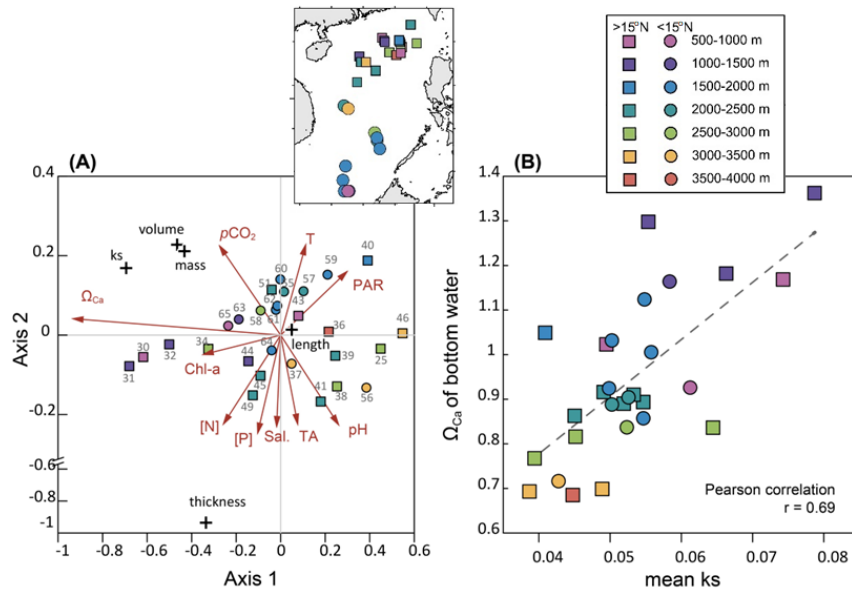
351

Figure 5. Redundancy analysis (RDA) ordinations for environmental variables and morphological measurements (A) and (B) linear correlation and correlation coefficient (p < 0.05) between Ω_{Ca} at bottom depths and mean ks from surface samples.

355

5. Discussion

5.1 ~~Comparations~~ Comparison between laboratory dissolution experiment and natural samples

In this study, we evaluate fossil coccolith responses to dissolution under laboratory experiments and field settings. In the dissolution experiment, ks values are higher than the modern coccoliths in the SCS due to the higher abundance of the relatively thicker *G. caribbeanica* in the downcore sediment sample. Though the absolute values of ks cannot be directly compared between the dissolution experiment (Fig. 2B) and surface sediments (Fig. 4A), the trajectory of morphological variations during the dissolution experiment does provide important diagnostic information to explain phenomena observed in the surface sediment samples.

First, the phenomenon that coccolith length increased with the decrease of ks could be observed in both the dissolution experiment (Fig. 2C) and natural surface sediments (Fig. 4B).

370 The laboratory experiment showed that under controlled conditions (known changes in water
371 chemistry and uniform species composition), the coccolith morphology variations (mean length
372 and mean ks) reflected different degrees of dissolution. We also observed a length-related
373 dissolution pattern, where smaller coccoliths gradually dissolve with the increase in Calgon®
374 concentration, leading to a higher average length but a lower mean ks. The mean ks and mean
375 length relationships in the surface samples (Fig. 4B) show a similar trend to the laboratory
376 observations (Fig. 2C). Thus, the observed trend and the largest size and lowest ks in the surface
377 sediment samples are explained by the dissolution of the smallest species due to the lower Ω_{Ca}
378 at the deepest samples and increasing the abundance of the larger coccoliths.

379 Second, changes in the σ/ks ratio in the dissolution experiment reflect a slight and
380 gradual increase in dissolution and then a decrease with the highest concentrations of Calgon®
381 (Fig. 2C). In the laboratory experiment, the subsample with no Calgon® solution presented well-
382 preserved coccoliths with high mean ks and a small standard deviation. As the amount of
383 Calgon® solution added to each subsample increases, small coccoliths start dissolving
384 preferentially, decreasing the mean ks and increasing the standard deviation (Fig. 2B). With
385 higher amounts of Calgon® solution (4 and 6 ml), the small coccoliths are completely dissolved,
386 resulting in an assemblage dominated by larger coccoliths (Fig. 2C). Under these highest
387 dissolution stages, the larger coccoliths are also partially dissolved then both mean ks and σ
388 decrease (Fig. 2B). In this way, the σ reflects how differential dissolution size selection affects
389 the composition of the assemblages. Hence, samples that are more (less) susceptible to
390 dissolution result in more homogeneous (heterogeneous) assemblages regarding carbonate
391 preservation.

392 However, the trajectory of σ/ks *vs.* ks in surface sediments seems more complex than in
393 the dissolution experiment (Fig. 4A). First, there is a group of samples with a positive correlation
394 between σ/ks and ks from shallow areas of the north and south SCS. The depth of samples from
395 northern and southern SCS regions is similar, so we argue that this feature is not caused by
396 dissolution but due to the ~~species~~ assemblage composition differences in both parts of the SCS.
397 The coccolithophores have multi-stage blooms in the north SCS, with a peak of *G. oceanica* in
398 late winter, when coccolithophore fluxes are highest due to strong water column mixing and
399 renewed nutrient inventory, and another of *E. huxleyi* in early spring (Chen et al., 2007; Jin et
400 al., 2019~~; Chen et al., 2007~~). In contrast, *E. huxleyi* is the dominant species in the more
401 oligotrophic south SCS (Fernando et al., 2007b) due to its higher competitiveness in situations
402 of lower nutrient concentration (particularly nitrate) compared to *G. oceanica* (Eppley et al.,
403 1969). So, even without any influence from dissolution, the ~~coccolith~~ assemblages in the north
404 SCS should feature a higher species diversity and, thereby, a higher σ/ks compared with the

405 coccolith in the south SCS. Hence, the variety of the coccolith assemblages in the surface

406 sediment samples results in different trajectories in σ/ks *vs*. ks plotting. These results highlight

407 the role of assemblage composition on the degree of dissolution as the large geographical

408 variability potentially influences the coccolithophore calcite production during its life cycle. But

409 the general trend of σ/ks *vs*. ks in surface sediment is still following the trends observed in the

410 dissolution experiment: (1) ks decreases with dissolution; (2) σ/ks increases slightly when

411 dissolution starts and (3) then it decreases with greater dissolution.

412

413 5.2 Sedimentary record of coccolith morphology: ~~life-cycle~~calcification *vs*.

414 dissolution factors

415 Previous studies have evaluated changes in the calcification of Noëlaerhabdaceae

416 coccoliths in glacial-interglacial cycles through analyses of the coccolith mass and attributed

417 morphological variations mainly to water column nutrient availability and carbonate chemistry

418 parameters, related to the coccolithophores life-cycle (e.g., Beaufort et al., 2011). Su et al.

419 (2020) found that the environmental dynamics of the surface photic zone controlled

420 Noëlaerhabdaceae coccoliths' calcification in northern SCS (MD05-2904). Similarly, higher

421 calcite production recorded by increased coccolith mass has been attributed to the increased

422 $[CO_3^{2-}]$ in the surface water column in the South Indian Ocean and North Atlantic Ocean in

423 modern sediments (Beaufort et al., 2011). Dissolution effects were thought to be less likely

424 drivers of changes in the morphology of coccolith (Beaufort et al., 2011; Su et al., 2020), which

425 is a reasonable assumption for the coccoliths depositing in shallow sediments above the

426 lysocline. These interpretations are partially sustained by the findings of Beaufort et al. (2007),

427 who found no significant coccolith dissolution during the settling in sediment traps deployed

428 between 250 and 2500 m. The former study proposed that most of the dissolution occurs in the

429 euphotic zone and possibly in the guts of grazers, therefore, discarding the impact of bottom

430 water chemistry and/or post-burial processes on coccolithophore weight.

431 In our set of samples in the SCS, the RDA results show that mean thickness and length

432 significantly correlate to nitrate and phosphate at 50 m (Table 2). This observation agrees with

433 Jin et al. (2016), who found that biometric attributes of *E. huxleyi* correlated with nutrient

434 concentrations in the plankton samples in the East China Sea (ECS). Nutrient variables are

435 important for coccolithophore calcification (Raven and Crawfurd, 2012) and morphological

436 parameters, at least in species of the Noëlaerhabdaceae family (Båtvik et al., 1997; Pasche et al.,

437 1998). However, based on the extended evidence of our study, including carbonate chemistry

438 at the depth of the sediment samples in the SCS, we observe evidence that several of the

439 morphological parameters measured are not only influenced by primary biomineralization. Still,

440   abiogenic post- or syn-depositional processes override this signal in the sediment samples in this

441   region. The highest correlations between coccolith morphology, namely mean ks, volume, and

442   thickness, with the bottom water calcite saturation, Ω_{Ca}, indicates that the calcium carbonate

443   preservation conditions could strongly override some of the morphological parameters in fossil

444   coccoliths (Table 2, Fig. 5A). We suggest that the mean ks of coccolith could be a potential proxy

445   for the carbonate dissolution in the bottom water, especially in sites near or below the

446   lyscocline.

447   Carbonate dissolution may also happen within the shallow sediment (Sulpis et al., 2021;

448   Subhas et al., 2022). Based on our current dataset and using only the morphological variations,

449   we cannot distinguish where the dissolution happens at the time of deposition in the sediment

450   water interface, or post-burial in the first cms of the seafloor sediment. For the deep ocean

451   depositions with lower sedimentary rates, such as the deepest parts of the SCS (Huang and

452   Wang, 2006), the exposure time of particles to bottom water should be longer than that along

453   the continental slope. Thus, we suggest that the major dissolution in the deep SCS happens on

454   the sediment-water boundary instead of within pore water. Interestingly, the ks of coccolith in

455   the surface sediment of the ECS are much lower, as low as 0.01 (Jin et al., 2019), than those in

456   our study, which is higher than 0.04. However, the ks of coccolith during the laboratory

457   dissolution experiment performed by Jin et al. (2019; Fig. 9A in that study) show the same range

458   as our measurements. The ECS samples are from the continental shelf with high sedimentary

459   rates and organic carbon content (Jin et al., 2019). In these settings, the coccoliths continuously

460   dissolve after being buried within the first centimeters of the seafloor sediments in response to

461   organic matter remineralization and CO_2 release, resulting in a ~30-50 % decrease in coccolith

462   mass (Jin et al., 2019). Therefore, the sedimentary environment has to be individually evaluated

463   to understand which process is controlling the dissolution of coccolithophores at the seafloor.

464   More detailed work, such as in-situ pore water chemistry measurements, would be necessary

465   to fully reveal the fate of coccolith dissolutions in different burial scenarios (Holcová and

466   Scheiner, 2022).

467   Among all the morphological parameters, we find the mean ks of coccolith as is a more

468   robust dissolution proxy compared to the other measured morphological parameters. Firstly,

469   we observe a higher correlation coefficient between mean ks of coccolith and Ω_{Ca} compared

470   with other morphological parameters. Secondly, although volume, mass, and thickness are also

471   highly correlated with Ω_{Ca}, these morphological parameters vary more with the feature of

472   different coccolithophores, including variations in coccolith circularity and cell sizes (Young and

473   Ziveri, 2000; Bolton et al., 2016). Thirdly, the thickness is a morphological pattern sensitive to

474   the upper ocean's preservation and surface ocean environmental nutrients conditions during

475 biomineralization (Table 2). Another important feature of ks is its high sensitivity to dissolution.
476 As shown in Fig. 4, the ks of coccolith have already begun to decrease even though the water
477 depths are only at ~2000 m, which is below the modern lysocline but above the CDD in the SCS
478 (Wang et al., 1995; Luo et al., 2018). Finally, the dissolution effects on morphological attributes
479 of mean ks agree well with the laboratory dissolution experiment, in which each subsample's
480 mean ks reflected different preservation stages (Fig. 3).

481 Despite a noticeable degree of uncertainty due to the mixing of life-cycle and post-
482 mortem signals in the sedimentary record, similar findings of calcite dissolution modifying
483 coccolith's morphology in waters at or below saturation suggest that the conclusions drawn
484 from the present study are not unique to the SCS. In the Sub-Antarctic and Antarctic zone,
485 dissolution signals affecting coccolithophores were manifested as a decrease in mass and distal
486 shield length of *E. huxleyi* coccoliths preserved in surface sediments (~~Vollmar et al., 2022;~~ Rigual-
487 Hernández et al., 2020b; Vollmar et al., 2022).   Based on this collective evidence, a key
488 reasonable question could be, "can the morphological variation of coccoliths be employed to
489 trace their evolution safely, or ~~could they~~instead be a good proxy for carbonate preservation"?
490

491 5.3. Implications for interpreting the downcore history of coccolithophore morphology

492 On longer time scales, the morphological variations of coccoliths have been employed
493 to trace coccolithophores evolutionary trends. Bolton et al. (2016) first measured the ks of
494 Noëlaerhabdaceae in the last 15 million years. They found that the decrease of coccolith ks
495 paralleled the reduction of atmospheric pCO_2 since the late Miocene and interpreted this as a
496 decrease in biomineralization. More recent works by Beaufort et al. (2022) and Jin et al. (2022b)
497 focused on the coccolithophore evolution over the last 2 million years by measuring coccolith
498 mass, highlighting the role of seasonality and local environments in the evolution and
499 production of Noëlaerhabdaceae. Similarly, Guitián et al. (2020) studied size trends across
500 different regions between Oligocene to the Early Miocene, concluding that cell size distribution
501 was controlled by multiple competing factors, with a strong selective pressure from CO_2 decline
502 as a potential mechanism. This study examined dissolution by looking, among others, at the
503 fragmentation and etching of coccoliths and found that temporal trends in lith size distributions
504 were not significantly affected. This agrees with our observations since the mean length in SCS
505 surface sediments does not correlate with any saturation state related parameter. However,
506 Guitián et al. (2022), using a new calibration in the C-Calcita software that enables estimations
507 of coccolith thickness up to 3.1 microns, found that elliptical ks (kse) was inversely correlated
508 with the relative abundance of dissolution-resistant nannoliths. This was interpreted as a
509 dissolution control on the elliptical shape factors in coccolithophores between Oligocene and

510 Miocene, as it was found in our surface sediment samples. Therefore, we propose that for

511 studies focusing on coccolithophores evolutionary histories, it would be safer to select a shallow

512 sediment core with low organic carbon content, high clay content, and always lying above the

513 carbonate lysocline (Guitián et al., 2020).

514 One useful way to identify dissolution in these studies covering geological time scales

515 could be plotting the σ/ks against ks. If an increase of σ/ks is detected in the sediment coccolith

516 without any significant variations in coccolith assemblage or with an increase of in dissolution-

517 resistant species (Guitián et al., 2022), it should be interpreted as a dissolution. Another way to

518 determine separate evolutionary/ecological influences on ks variations could be to measure the

519 ks of coccolith across a close spatial gradient which includes different depositional depths.

520 Significant variations in the morphological attributes of the fossil coccolithophores would likely

521 be caused by different saturation through time at different sites. Related to this last suggestion,

522 coupling downcore morphological assessment in coccolithophores with other calcareous

523 proxies measurements, such as size-normalized weight of planktic foraminiferal tests (Lohman,

524 1995; Broecker and Clark, 2001; Barker et al., 2002), which include recent advances in

525 morphological analyses in large microfossils (Iwasaki et al., 2015; 2019), may provide an even

526 more precise and safe quantitative estimates of past deep-carbonate chemistry parameters.

6. Summary

528 This study demonstrates, based on morphological attributes of *E. huxleyi* and

529 *Gephyrocapsa* spp. (> 2 μm), that dissolution effects primarily affect the morphology of

530 coccoliths preserved in the deep ocean. In the SCS surface sediments, bottom water Ω_{ca}

531 saturation plays a major role in the variation of the coccoliths' ks shape factor, which has the

532 potential, based on the current calibration, to quantitatively reconstruct past carbonate

533 dissolution changes. Our laboratory-controlled dissolution results show that the mean ks

534 decreased in response to increased amounts of corrosive solution. We propose the ratio σ/ks

535 *vs*. mean ks to evaluate the degree of dissolution (light, strong, or no dissolution) occurring in

536 the sedimentary record. A length-related dissolution pattern was also observed in the laboratory

537 and surface sediments, with small coccoliths more prone to suffer dissolution, increasing larger

538 coccolith specimens and affecting the assemblage composition. As in the laboratory experiment,

539 the coccolith's ks from surface sediments decreased with dissolution, and the σ/ks trajectory

540 reflected different dissolution stages. However, the σ/ks in surface sediment showed a more

541 complex response due to the natural variability of the surface sediment samples in terms of

542 geographical differences in multiple environmental factors. These findings demonstrate that,

543 despite the complexity complementary of the carbonate system and ecological aspects, the

coccoliths ks factor allied to σ/ks ratio has potential as a dissolution proxy to track changes in the seafloor carbonate saturation state. Although a stable proxy, the mean ks should be applied with caution, particularly when applied to longer time scales, in which evolutionary trends might exert control on morphological attributes of fossil coccolithophores.

Author contributions
AG, HZ, RHN and IHA conceived and designed the study. AG and HZ conducted the lab work and sample analyses. AG, HZ and IHA performed the statistical analysis. AG, HZ and IHA wrote the manuscript with substantial contributions from all co-authors.

Competing interests
The authors declare that they have no conflict of interest.

Data availability
Research data is available as supplementary material and in the Zenodo (https://doi.org/10.5281/zenodo.7271441, Gerotto et al., 2022) and PANGAEA (https://doi.pangaea.de/10.1594/PANGAEA.954015 and https://doi.pangaea.de/10.1594/PANGAEA.954016, Gerotto et al., 2023a,bpending doi) data repositories.

Acknowledgments
This study was financed in part by the Coordenação de Aperfeiçoamento de Pessoal de Nível Superior - Brasil (CAPES) - Finance Code 001 to A.G. and the ETH Core and Swiss National Science Foundation (Award 200021_182070) funding to H. M. Stoll. Additional funding was provided by the National Natural Science Foundation of China (grants 42188102 and 41930536) to C.L. Thanks also to the International Ocean Discovery program for providing the sample used for the dissolution experiment.

References
Archer, D., Winguth, A., Lea, D., and Mahowald, N. What caused the glacial/interglacial atmospheric pCO_2 cycles? Rev. Geophys., 38 (2)(1999), 159–189, https://doi.org/10.1029/1999RG000066, 2000.

Barker, S., and Elderfield, H. Foraminiferal calcification response to glacial-interglacial changes in atmospheric CO_2, Science, 297(5582), 833-836, https://doi.org/10.1126/science.1072815, 2002.

574 Båtvik, H., Heimdal, B. R., Fagerbakke, K. M., Green, J. C. Effects of unbalanced nutrient regime
575   on coccolith morphology and size in *Emiliania huxleyi* (Prymnesiophyceae), Eur. J.
576   Phycol., 32(2), 155–165, https://doi.org/10.1080/09670269710001737089, 1997.

577 Beaufort, L. Weight estimates of coccoliths using the optical properties (birefringence) of calcite,
578   Micropaleontology, 51(4), 289-297, https://doi.org/10.2113/gsmicropal.51.4.289,
579   2005.

580 Beaufort, L., Gally, Y., Suchéras-Marx, B., Ferrand, P., and Duboisset, J. A universal method for
581   measuring the thickness of microscopic calcite crystals, based on ~~B~~bidirectional ~~C~~circular
582   ~~P~~polarization, Biogeosciences, 18~~ ~~(3), 775-785, https://doi.org/10.5194/bg-18-775-
583   2021, 2021.

584 Beaufort, L., Probert, I., De Garidel-Thoron, T., Bendif, E. M., Ruiz-Pino, D., Metzl, N., et al.
585   Sensitivity of coccolithophores to carbonate chemistry and ocean acidification, Nature,
586   476(7358), 80–83, https://doi.org/10.1038/nature10295, 2011.

587 Beaufort, L., Probert, I., and Buchet, N. Effects of acidification and primary production on
588   coccolith weight: Implications for carbonate transfer from the surface to the deep
589   ocean, Geochem., Geophy., Geosy., 8(8), 1–18,
590   https://doi.org/10.1029/2006GC001493, 2007.

591 Beaufort, L., Bolton, C. T., Sarr, A. C., et al. Cyclic evolution of phytoplankton forced by changes
592   in tropical seasonality, Nature, 601, 79–84, https://doi.org/10.1038/s41586-021-04195-
593   7, 2022.

594 Bollmann, J. Weight approximation of coccoliths using a circular polarizer and interference
595   colour derived retardation estimates – (The CPR Method), Biogeosciences, 11, 1899-
596   1910, https://doi.org/10.5194/bg-11-1899-2014, 2014.

597 Bollmann, J., Herrle, J. O. Morphological variation of *Emiliania huxleyi* and sea surface salinity,
598   Earth Planet. Sc. Lett., 255(3-4), 273–288, https://doi.org/10.1016/j.epsl.2006.12.029,
599   2007.

600 Bolton, C. T., Hernández-Sánchez, M. T., Fuertes, M. Á., González-Lemos, S., Abrevaya, L.,
601   Mendez-Vicente, A., et al. Decrease in coccolithophore calcification and CO_2 since the
602   middle Miocene, ~~Nature~~ Nat. ~~Communications~~Commun., 7, 10284,
603   https://doi.org/10.1038/ncomms10284, 2016.

604 Bordiga, M., Bartol, M., Henderiks, J. Absolute nannofossil abundance estimates: 314
605   Quantifying the pros and cons of different techniques, Rev. de Micropaleontol., 58, 155-
606   165, https://doi:10.1016/j.revmic.2015.05.002, 2015.

607 Broecker, W. S., and Clark, E. Glacial-to-Holocene Redistribution of Carbonate Ion in the Deep
608   Sea, Science, 294(5549), 2152–2155, http://www.jstor.org/stable/3085356, 2001.

Formatado: Fonte: Itálico

609   Broerse, A. T. C., Ziveri, P., and Honjo, S. Coccolithophore (-CaCO$_3$) flux in the Sea of Okhotsk:
610   Seasonality, settling and alteration processes, Mar. Micropaleontol., 39(1–4), 179–200,
611   https://doi.org/10.1016/S0377-8398(00)00020-7, 2000.

612   Buiteveld, H. A model for calculation of diffuse light attenuation (PAR) and Secchi depth, Neth.
613   J. Aquat. Ecol., 29, 55–65, https://doi.org/10.1007/BF02061789, 1995.

614   Charalampopoulou, A., Poulton, A. J., Bakker, D. C. E., Lucas, M. I., Stinchcombe, M. C., Tyrrell,
615   T. Environmental drivers of coccolithophore abundance and calcification across Drake
616   Passage (Southern Ocean), Biogeosciences, 13, 5917–5935, https://doi.org/10.5194/bg-
617   13-5917-2016, 2016.

618   Chen, C. T. A., Wang, S. L., Chou, W. C., and Sheu, D. D. Carbonate chemistry and projected future
619   changes in pH and CaCO3 saturation state of the South China Sea, Mar. Chem., 101(3–
620   4), 277–305, https://doi.org/10.1016/j.marchem.2006.01.007, 2006.

621   Chen, C. T. A., Wang, S. L., Wang, B. J., and Pai, S. C. Nutrient budgets for the South China sea
622   basin, Mar. Chem., 75(4), 281–300, https://doi.org/10.1016/S0304-4203(01)00041-X,
623   2001.

624   Chen, Y. L. L. Spatial and seasonal variations of nitrate-based new production and primary
625   production in the South China Sea, Deep-Sea Res. Pt. I, 52(2), 319–340,
626   https://doi.org/10.1016/j.dsr.2004.11.001, 2005.

627   Chen, Y. L. L., Chen, H. Y., and Chung, C. W. Seasonal variability of coccolithophore abundance
628   and assemblage in the northern South China Sea, Deep-Sea Res. Pt. II: Top. Stud.
629   Oceanogr., 54(14–15), 1617–1633, https://doi.org/10.1016/j.dsr2.2007.05.005, 2007.

630   Chou, W. C., Sheu, D. D., Lee, B. S., Tseng, C. M., Chen, C. T. A., Wang, S. L., and Wong, G. T. F.
631   Depth distributions of alkalinity, TCO$_2$ and δ^{13} CTCO$_2$ at SEATS time-series site in the
632   northern South China Sea, Deep-Sea Res. Pt. II: Top. Stud. Oceanogr., 54(14–15), 1469–
633   1485, https://doi.org/10.1016/j.dsr2.2007.05.002, 2007.

634   Conkright, M. E., Locarnini, R. A., Garcia, H. E., O'Brien, T. D., Boyer, T. P., Stephens, C., Antonov,
635   J. I. World Ocean Atlas 2001: Objective Analyses, Data Statistics, and Figures, CD-ROM
636   Documentation. National Oceanographic Data Center, Silver Spring, MD, 17 pp, 2002.

637   Emerson, S. R., and Archer, D. Calcium carbonate preservation in the ocean. Philos. Tr. R. Soc. S-
638   A., 331(1616), 29–40, https://doi.org/10.1098/rsta.1990.0054, 1990.

639   Eppley, R. W., Rogers, J. N., and Mccarthy, J. J. Half-saturation constants for uptake of nitrate
640   and ammonia, Liminol. Oceanogr., 14(6), 912–920,
641   https://doi.org/10.4319/lo.1969.14.6.0912, 1969.

Feldmeijer, W., Metcalfe, B., Scussolini, P., and Arthur, K. The effect of chemical pretreatment of sediment upon foraminiferal-based proxies, Geochem., Geophy., Geosy., 14(10), 3996-4014, https://doi.org/10.1002/ggge.20233, 2013.

Fernando, A. G. S, Peleo-Alampay, A. M., Lucero, E. S., and Wiesner, M. G. Surface sediment distribution of *Florisphaera profunda* in the South China Sea: an effect of dissolution? J. Nannoplankton Res., 29(2), 102–07, 2007a.

Fernando, A. G. S., Peleo-Alampay, A. M., and Wiesner, M. G. Calcareous nannofossils in surface sediments of the eastern and western South China Sea, Mar. Micropaleontol., 66, 1–26, https://doi.org/10.1016/j.marmicro.2007.07.003, 2007b.

Flores, J. A., Marino, M., Sierro, F. J., Hodell, D. A., and Charles, C. D. Calcareous plankton dissolution pattern and coccolithophore assemblages during the last 600 kyr at ODP Site 1089 (Cape Basin, South Atlantic): Paleoceanographic implications. Palaeogeogr Palaeocl, 196(3–4), 409–426, https://doi.org/10.1016/S0031-0182(03)00467-X, 2003.

Fuertes, M. Á., Flores, J. A., and Sierro, F. J. The use of circularly polarized light for biometry, identification and estimation of mass of coccoliths, Mar. Micropaleontol., 113, 44–55, https://doi.org/10.1016/j.marmicro.2014.08.007, 2014.

Gerotto, A., Zhang, H., Nagai, R. H., Stoll, H. M., Figueira, R. C. L., Chuanlian, L., Hernández-Almeida, I. Morphological measurements of coccoliths from surface samples of South China Sea, Zenodo [data set], https://doi.org/10.5281/zenodo.7271441, 2022.

Gerotto, A., Zhang, H., Nagai, R. H., Stoll, H. M., Figueira, R. C. L., Chuanlian, L., Hernández-Almeida, I. Morphological measurements of coccoliths from surface samples of R/V SONNE cruise SO95. PANGAEA, https://doi.pangaea.de/10.1594/PANGAEA.954015, 2023a.

Gerotto, A., Zhang, H., Nagai, R. H., Stoll, H. M., Figueira, R. C. L., Chuanlian, L., Hernández-Almeida, I. Coccolith dissolution experiment from one sample of ODP Hole 130-807A. PANGAEA, https://doi.pangaea.de/10.1594/PANGAEA.954016, 2023b.

González-Lemos, S., Guitián, J., Fuertes, M. Á., Flores, J. A., and Stoll, H. M. Technical note: An empirical method for absolute calibration of coccolith thickness, Biogeosciences, 15(4), 1079–1091, https://doi.org/10.5194/bg-15-1079-2018, 2018.

Goyet, C., Healy, R. J., and Ryan, J. P. Global distribution of total inorganic carbon and total alkalinity below the deepest winter mixed layer depths. ORNL/CDIAC-127, NDP-076. Carbon Dioxide Information Analysis Center, Oak Ridge National Laboratory, U.S. Department of Energy, Oak Ridge, Tennessee, 2000.

675 Guitián, J., Dunkley Jones, T., Hernández-Almeida, I., Löffel, T., and Stoll, H. M. Adaptations of
676   coccolithophore size to selective pressures during the Oligocene to Early Miocene high
677   CO2 world, Paleoceanogr. and Paleoclimatology, 35(12), e2020PA003918,
678   https://doi.org/10.1029/2020PA003918, 2020.

679 Guitián, J., Fuertes, M. Á., Flores, J. A., Hernández-Almeida, I., and Stoll, H. Variation in
680   calcification of Reticulofenestra coccoliths over the Oligocene-Early Miocene, Biogeosci.
681   Discuss., 1-17, https://doi.org/10.5194/bg-19-5007-2022https://doi.org/10.5194/bg-
682   2022-66, 2022.

683 Hammer, Ø., Harper, D. A. T., Ryan, P. D. PAST: Paleontological Statistics Software Package for
684   Education and Data Analysis, Palaeonto. Electron., 4(1), 1–9,
685   doi.org/10.1016/j.bcp.2008.05.025, 2001.

686 Hay, W. W. Carbonate fluxes and calcareous nannoplankton.
687   H. Thierstein, J. Young (Eds.), Coccolithophores: From Molecular Processes to Global
688   Impact, Springer, Berlin (2004), pp. 509-528, 2004.

689 Henderiks, J., and Pagani, M. Refining ancient carbon dioxide estimates: Significance of
690   coccolithophore cell size for alkenone-based pCO_2 records, Paleoceanography, 22(3), 1–
691   12, https://doi.org/10.1029/2006PA001399, 2007.

692 Hernández, A. S. R., Trull, T. W., Nodder, S. D., Flores, J. A., Bostock, H., Abrantes, F., et al.
693   Coccolithophore biodiversity controls carbonate export in the Southern Ocean,
694   Biogeosciences, 17(1), 245–263, https://doi.org/10.5194/bg-17-245-2020, 2020.

695 Holcová, K., and Scheiner, F. An experimental study on post-mortem dissolution and overgrowth
696   processes affecting coccolith assemblages: A rapid and complex process, Geobiology,
697   (September)00, 1–17, https://doi.org/10.1111/gbi.12528, 2022.

698 Hönisch, B., Ridgwell, A., Schmidt, D. N., Thomas, E., Gibbs, S. J., Sluijs, A., et al. The geological
699   record of ocean acidification, Science, 335(6072), 1058–1063,
700   https://doi.org/10.1126/science.1208277, 2012.

701 Huang, W., and Wang, P. Sediment mass and distribution in the South China Sea since the
702   Oligocene. Sci. China Ser. D Earth Sci. 49, 1147–1155. https://doi:10.1007/s11430-006-
703   2019-4, 2006.

704 Iglesias-Rodriguez, M. D., Halloran, P. R., Rickaby, R. E. M., Hall, I. R., Colmenero-Hidalgo, E.,
705   Gittins, J. R., et al. Phytoplankton calcification in a high-CO_2 world, Science, 320(5874),
706   336–340, https://doi.org/10.1126/science.1154122, 2008.

707 IPCC: Climate Change and Land: an IPCC special report on climate change, desertification, land
708   degradation, sustainable land management, food security, and greenhouse gas fluxes in

709   terrestrial ecosystems [P.R. Shukla, J. Skea, E. Calvo Buendia, V. Masson-Delmotte, H.-
710   O. Pörtner, D. C. Roberts, P. Zhai, R. Slade, S. Connors, R. van Diemen, M. Ferrat, E.
711   Haughey, S. Luz, S. Neogi, M. Pathak, J. Petzold, J. Portugal Pereira, P. Vyas, E. Huntley,
712   K. Kissick, M. Belkacemi, J. Malley, (eds.)]. In press, 2019.

713 Iwasaki, S., Kimoto, K., Okazaki, Y., and Ikehara, M. Micro-CT ~~S~~scanning of ~~T~~tests of ~~T~~three
714   ~~P~~planktic ~~F~~foraminiferal ~~S~~species to ~~C~~clarify ~~D~~dissolution ~~P~~process and
715   ~~P~~progress, Geochem., Geophy., Geosy., 20(12), 6051-6065,
716   https://doi.org/10.1029/2019GC008456, 2019.

717 Iwasaki, S., Kimoto, K., Sasaki, O., Kano, H., Honda, M. C., and Okazaki, Y. Observation of the
718   dissolution process of *Globigerina bulloides* tests (planktic foraminifera) by X-ray
719   microcomputed tomography, Paleoceanography, 30(4), 317-331,
720   https://doi.org/10.1002/2014PA002639, 2015.

721 Johnsen, S. L., and Bollmann, J. Segmentation, retardation and mass approximation of
722   birefringent particles on a standard light microscope, J. Microsc., 280, 30-50,
723   https://doi.org/10.1111/jmi.12932, 2020.

724 Jin, X., Liu, C., Poulton, A. J., Dai, M., and Guo, X. Coccolithophore responses to environmental
725   variability in the South China Sea: Species composition and calcite content,
726   Biogeosciences, 13(16), 4843–4861, https://doi.org/10.5194/bg-13-4843-2016, 2016.

727 Jin, X., Liu, C., Xu, J., and Guo, X. Coccolithophore ~~A~~abundance, ~~Degree~~ degree of ~~C~~calcification,
728   and ~~Their~~ their ~~Contribution~~ contribution to ~~Particulate~~ particulate ~~I~~inorganic ~~C~~carbon
729   in the South China Sea, J. Geophys. Res-Biogeo., 127(4), e2021JG006657,
730   https://doi.org/10.1029/2021JG006657, 2022a.

731 Jin, X., Liu, C., and Zhang, H. Coccolith morphological and assemblage responses to dissolution
732   in the recent sediments of the East China Sea, Mar. Micropaleontol., 152~~(January 2018)~~,
733   101709, https://doi.org/10.1016/j.marmicro.2018.09.001, 2019.

734 Jin, X., Ma, W., and Liu, C. Origin of the long-term increase in coccolith size and its implication
735   for carbon cycle and climate over the past 2 Myr, Quaternary Sci. Rev., 290, 107642,
736   https://doi.org/10.1016/j.quascirev.2022.107642, 2022b.

737 Le, J., and Shackleton, N. J. Carbonate dissolution fluctuations in the western equatorial Pacific
738   during the late Quaternary, Paleoceanography, 7, 21–42,
739   https://doi.org/10.1029/91PA02854, 1992.

740 Libes, S. M. An Introduction to Marine Biogeochemistry, 2nd ed. Burlington, MA:
741   Academic Press Noone, K., Sumaila, R.; Diaz R.J. (eds) 2009. Valuing the
742   Oceans, Stockholm Environmental Institute, 2009.

743 Lin, J., Lee, Z., Ondrusek, M., and Du, K. Remote sensing of normalized diffuse
744   attenuation coefficient of downwelling irradiance, J. Geophys. Res-Oceans, 121(9),
745   6717-6730, https://doi.org/10.1002/2016JC011895, 2016.

746 Liu, J., Xiang, R., Chen, M., Chen, Z., Yan, W., and Liu, F. Influence of the Kuroshio current
747   intrusion on depositional environment in the Northern South China Sea: Evidence from
748   surface sediment records, Mar. Geol., 285(1–4), 59–68,
749   https://doi.org/10.1016/j.margeo.2011.05.010, 2011.

750 Lohman, G. P. A model for variation in the chemistry of planktonic foraminifera due to secondary
751   calcification and selective dissolution, Paleoceanogr. Paleoclimatol., 10(3), 445-457,
752   https://doi.org/10.1029/95PA00059, 1995.

753 Luo, Y., Kienast, M., and Boudreau, B. P. Invariance of the carbonate chemistry of the South
754   China Sea from the glacial period to the Holocene and its implications to the Pacific
755   Ocean carbonate system, Earth Planet. Sci. Lett., 492, 112–120,
756   https://doi.org/10.1016/j.epsl.2018.04.005, 2018.

757 Marsaglia, K., Milliken, K., Leckie, R., M., Tentori, D., Doran, L. IODP Smear Slide Digital Reference
758   for Sediment Analysis of Marine Mud. Part 2: Methodology and Atlas of Biogenic
759   Components. IODP Technical Note 2, doi:10.14379/iodp.tn.2.2015, 2015.

760 Murtugudde, R., Beauchamp, J., McClain, C. R., Lewis, M., and Busalacchi, A. Effects of
761   penetrative radiation on the upper tropical ocean circulation, J. Climate, 15(5), 470-486,
762   https://doi.org/10.1175/1520-0442(2002)015<0470:EOPROT>2.0.CO;2, 2002.

763 Paasche, E. Roles of nitrogen and phosphorus in coccolith formation in *Emiliania huxleyi*
764   (Prymnesiophyceae), Eur. J. Phycol., 33(1), 33-42,
765   https://doi.org/10.1080/09670269810001736513, 1998.

766 Pälike, H., Lyle, M. W., Nishi, H., Raffi, I., Ridgwell, A., Gamage, K., et al. A Cenozoic record of the
767   equatorial Pacific carbonate compensation depth, Nature, 488(7413), 609–614,
768   https://doi.org/10.1038/nature11360, 2012.

769 Pälike, H., Norris, R. D., Herrle, J. O., Wilson, P. A., Helen, K., Lear, C. H., et al. The heartbeat of
770   the Oligocene climate system, Science, 314(5807), 1894–1898,
771   https://www.jstor.org/stable/20035092, 2006.

772 Pierrot, D., Lewis, E., and Wallace, D. W. R. MS Excel Program Developed for CO_2 System
773   Calculations - version 2.1. ORNL/CDIAC-105a. Carbon Dioxide Information Analysis
774   Center, Oak Ridge National Laboratory, U.S. Department of Energy, Oak Ridge,
775   Tennessee, https://doi.org/10.3334/CDIAC/otg.CO2SYS_XLS_CDIAC105a, 2012.

776 Pinxian, W., Qiubao, M., Yunhua, B., and Wenke, F. Planktonic foraminifera in the continental
777   slope of the northern South China Sea during the last 130,000 years and their

Ppaleo-Ooceanographic Iimplications, Acta Geol. Sin-Engl., 60(3), 1–11, https://doi.org/10.1111/j.1755-6724.1986.mp60003001.x, 1986.

Qu, T., Girton, J. B., and Whitehead, J. A. Deepwater overflow through Luzon Strait, J. Geophys. Res., 111(C1), C01002, https://doi.org/10.1029/2005JC003139, 2006.

Qu, T., Song, Y. T., and Yamagata, T. An introduction to the South China Sea throughflow: Its dynamics, variability, and application for climate, Dynam. Atmos. Oceans, 47(1–3), 3–14, https://doi.org/10.1016/j.dynatmoce.2008.05.001, 2009.

Rae, J. W. B., Zhang, Y. G., Liu, X., Foster, G. L., Stoll, H. M., and Whiteford, R. D. M. Atmospheric CO_2 over the Ppast 66 Mmillion Yyears from Mmarine Aarchives, Annu. Rev. Earth Pl. Sc., 49, 609–641, https://doi.org/10.1146/annurev-earth-082420-063026, 2021.

Raven, J. A., and Crawfurd, K. Environmental controls on coccolithophore calcification. Mar. Ecol. Prog. Ser., 470, 137–166. http://www.jstor.org/stable/24876210, 2012.

Rickaby, R. E. M., Bard, E., Sonzogni, C., Rostek, F., Beaufort, L., Barker, S., et al. Coccolith chemistry reveals secular variations in the global ocean carbon cycle? Earth Planet. Sci. Lett., 253(1–2), 83–95, https://doi.org/10.1016/j.epsl.2006.10.016, 2007.

Ridgwell, A., and Zeebe, R. E. The role of the global carbonate cycle in the regulation and evolution of the Earth system, Earth Planet. Sci. Lett., 234(3–4), 299–315, https://doi.org/10.1016/j.epsl.2005.03.006, 2005.

Riebesell, U., Zondervan, I., Rost, B., Tortell, P. D, Zeebe, R. E., and Morel, F. M. M. Reduced calcification of marine plankton in response to increased atmospheric CO_2, Nature, 407, 364–367, https://doi.org/10.1038/35030078, 2000.

Rigual-Hernández, A. S., Sánchez-Santos, J. M., Eriksen, R., Moy, A. D., Sierro, F. J., Flores, J. A., et al. Limited variability in the phytoplankton *Emiliania huxleyi* since the pre-industrial era in the Subantarctic Southern Ocean. Anthropocene, 31, 100254, https://doi.org/10.1016/j.ancene.2020.100254, 2020b.

Rigual Hernández, A. S., Trull, T. W., Nodder, S. D., Flores, J. A., Bostock, H., Abrantes, F., Eriksen, R.S., Sierro, F. J., Davies, D. M., Ballegeer, A.-M., Fuertes, M. A., and Northcote, L. C. Coccolithophore biodiversity controls carbonate export in the Southern Ocean, Biogeosciences, 17, 245–263, https://doi.org/10.5194/bg-17-245-2020, 2020a.

Roth, P. H., and Berger, W. H. Distribution and dissolution of coccoliths in the South and Central Pacific. Sliter, W. V., Be′ A. W. H., Berger, W. H. (Eds.), Dissolution of Deep-Sea Carbonates, Cushman Foundation Foraminiferal Research, Spec. Publ., N. 13, pp. 87-113, 1975.

Formatado: Fonte: Itálico

811 Roth, P. H., and Coulbourn, W. T. Floral and solution patterns of coccoliths in surface sediments
812 of the North Pacific. ~~Marine~~ Mar. ~~Micropaleontology~~Micropaleontol., 7(1), 1-52,
813 https://doi.org/10.1016/0377-8398(82)90014-7, 1982.

814 Sarmiento, J. L., Gruber, N. Ocean Biogeochemical dynamics. Princeton, NJ, Woodstock:
815 Princeton University Press. 528 pp, 2006.

816 Schlitzer, R. Ocean data View. Available at:<htt://odv.awi.de>, 2019.

817 Stoll, H. M., Ziveri, P. Separation of monospecific and restricted coccolith assemblages from
818 sediments using differential settling velocity, Mar. Micropaleontol., 46(1–2), 209-221,
819 https://doi.org/10.1016/S0377-8398(02)00040-3, 2002.

820 Su, X., Liu, C., and Beaufort, L. Late Quaternary coccolith weight variations in the northern South
821 China Sea and their environmental controls, Mar. Micropaleontol., 154, 101798,
822 https://doi.org/10.1016/j.marmicro.2019.101798, 2020.

823 Subhas, A. V., Dong, S., Naviaux, J. D., Rollins, N. E., Ziveri, P., Gray, W., et al. Shallow ~~C~~calcium
824 ~~C~~carbonate ~~C~~cycling in the North Pacific Ocean, Global Biogeochem. Cy., 36(5), 1–22,
825 https://doi.org/10.1029/2022GB007388, 2022.

826 Sulpis, O., Boudreau, B. P., Mucci, A., Jenkins, C., Trossman, D. S., Arbic, B. K., and Key, R. M.
827 Current $CaCO_3$ dissolution at the seafloor caused by anthropogenic CO_2, P. Natl. Acad.
828 Sci. USA, 115(46), 11700–11705, https://doi.org/10.1073/pnas.1804250115, 2018.

829 Sulpis, O., Jeansson E., Dinauer A., Lauvset, S. K., and Middelburg, J. J. Calcium carbonate
830 dissolution patterns in the ocean, Nat. Geosci., 14(6), 423–428,
831 http://dx.doi.org/10.1038/s41561-021-00743-y, 2021.

832 Thunell, R. C., Qingmin, M., Calvert, S. E., and Pedersen, T. F. Glacial-Holocene ~~B~~biogenic
833 ~~S~~sedimentation ~~P~~patterns in the South China Sea: Productivity ~~V~~variations and ~~S~~surface
834 ~~W~~water pCO_2, Paleoceanography, 7(2), 143–162, https://doi.org/10.1029/92PA00278,
835 1992.

836 Tian, J., Huang, E., and Pak, D. K. East Asian winter monsoon variability over the last glacial cycle:
837 Insights from a latitudinal sea-surface temperature gradient across the South China Sea,
838 Palaeogeogr. Palaeocl., 292(1–2), 319–324,
839 https://doi.org/10.1016/j.palaeo.2010.04.005, 2010.

840 USGCRP. Climate Science Special Report: Fourth National Climate Assessment, Volume I
841 [Wuebbles, D. J., ~~D.W.~~ Fahey, D. W., ~~K.A.~~ Hibbard, K. A., ~~D.J.~~ Dokken, D. J., ~~B.C.~~ Stewart,
842 B. C., and ~~T.K.~~ Maycock, T. K. (eds.)]. U.S. Global Change Research Program, Washington,
843 DC, USA, 470 pp., 2017.

844 Vollmar, N. M., Baumann, K. H., Saavedra-Pellitero, M., and Hernández-Almeida, I. Distribution
845 of coccoliths in surface sediments across the Drake Passage and calcification of *Emiliania*

846   *huxleyi* morphotypes, Biogeosciences, 19(3), 585–612, https://doi.org/10.5194/bg-19-
847   585-2022, 2022.

848   Wan, S., and Jian, Z. Deep water exchanges between the South China Sea and the Pacific since
849   the   last   glacial   period,   Paleoceanography,   29(12),   1162–1178,
850   https://doi.org/10.1002/2013PA002578, 2014.

851   Wan, S., Jian, Z., and Dang, H. Deep H̶hydrography of the South China Sea and D̶deep W̶water
852   C̶circulation in the Pacific S̶since the Last Glacial Maximum, Geochem., Geophy., Geosy.,
853   19(5), 1447–1463, https://doi.org/10.1029/2017GC007377, 2018.

854   Wan, S., Jian, Z., Gong, X., Dang, H., Wu, J., and Qiao, P. Deep water $[CO_3^{2-}]$ and circulation in
855   the s̶South China s̶Sea over the last glacial cycle, Quat. Sci. Rev., 243, 106499,
856   https://doi.org/10.1016/j.quascirev.2020.106499, 2020.

857   Wang, N., Huang, B.-Q., and Li, H. Deep-water carbonate dissolution in the northern South China
858   Sea   during   Marine   Isotope   Stage   3,   J.   Palaeogeogr.,   5(1),   100–107,
859   https://doi.org/10.1016/j.jop.2015.11.004, 2016.

860   Wang, P., Li, Q., and Dai, M. The South China Sea Deep: Introduction, Deep-Sea Res. Pt. II: Top.
861   Stud. Oceanogr, 122, 1-5, https://doi.org/10.1016/j.dsr2.2015.11.004, 2015.

862   Wang, P., Wang, L., Bian, Y., and Jian, Z. Late Quaternary paleoceanography of the South China
863   Sea: surface circulation and carbonate cycles, Mar. Geol., 127(1–4), 145–165,
864   https://doi.org/10.1016/0025-3227(95)00008-M, 1995.

865   Wang, P. X., and Li, Q. Y. The South China Sea: Paleoceanography and Sedimentology. Springer,
866   Berlin, Heidelberg, New York, p. 506, 2009.

867   Young, J. R., and Ziveri, P. Calculation of coccolith volume and its use in calibration of carbonate
868   flux estimates, Deep-Sea Res. Pt. II: Top. Stud. Oceanogr., 47(9–11), 1679–1700,
869   https://doi.org/10.1016/S0967-0645(00)00003-5, 2000.

870   Yu, J., and Elderfield, H. Benthic foraminiferal B/Ca ratios reflect deep water carbonate
871   saturation   state,   Earth   Planet.   Sci.   Lett.,   258(1–2),   73–86,
872   https://doi.org/10.1016/j.epsl.2007.03.025, 2007.

873   Yu, J., Menviel, L., Jin, Z. D., Thornalley, D. J. R., S. Barker, S., Marino, G., et al. Sequestration of
874   carbon in the deep Atlantic during the last glaciation, Nat. Geosci., 9, 319-324,
875   https://doi.org/10.1038/ngeo2657, 2016.

876   Zachos, J. C., Röhl, U., Schellenberg, S. A., Sluijs, A., Hodell, D. A., Kelly, D. C., et al. Paleoclimate:
877   Rapid acidification of the ocean during the p̶Paleocene-e̶Eocene thermal maximum,
878   Science, 308(5728), 1611–1615, https://doi.org/10.1126/science.1109004, 2005.

879   Zhang, H., Liu, C., Jin, X., Shi, J., Zhao, S., and Jian, Z. Dynamics of primary productivity in the
880   northern South China Sea over the past 24,000 years, Geochem., Geophy., Geosy.,
881   17(12), 4878–4891, https://doi.org/10.1002/2016GC006602, 2016.

882